Engineering Structures 221 (2020) 111101

Contents lists available at ScienceDirect

Engineering Structures

journal homepage: www.elsevier.com/locate/engstruct

Observations and analysis of wind pressures on the floor underside of elevated buildings

Jae H. Kim[a,*], Mohammadtaghi Moravej[b], Elaina J. Sutley[a], Arindam Chowdhury[c], Thang N. Dao[d]

[a] Department of Civil, Environmental, and Architectural Engineering, University of Kansas, 1520 W. 15th Street, Lawrence, KS 66045, United States
[b] Walker Consultants, 606 S Olive Street, #1100, Los Angeles, CA 90014, United States
[c] Department of Civil and Environmental Engineering, Florida International University, 10555 W. Flagler Street, EC 3680, Miami, FL 33174, United States
[d] Department of Civil, Construction and Environmental Engineering, University of Alabama, 24 7th Avenue, Tuscaloosa, AL 35487, United States

ARTICLE INFO

Keywords:
Elevated buildings
Wind engineering
Hurricane Michael
Wall of Wind

ABSTRACT

A popular method of building flood-proofing in coastal regions is the use of stilts or piers to elevate buildings. These elevated building structures are generally well-designed to reduce or withstand the hydrodynamic loading resulting from flooding waters, storm surge and carried debris. However, design for wind loading on elevated buildings is not well-informed or codified, despite the changes in the elevated buildings' aerodynamics. In order to begin developing the body of knowledge regarding wind effects on elevated buildings, a field study on such structures in the coastal region of the Florida Panhandle was conducted following 2018 Hurricane Michael. In addition, wind tunnel testing on large-scale models of an elevated single-story residential home was performed at the NHERI Wall of Wind Experimental Facility at the Florida International University. The evidence of floor underside damage from the field study are consistent with trends of pressure patterns from the experimental program. Measured pressure coefficients on the underside of wind tunnel models were significant and frequently of similar or greater magnitude to those on the roof, the latter for which estimation procedures have already been well-established. These findings show that deliberate design for floor underside pressures are necessary, and provide critical impetus for continued research in order to reduce damages observed in past hurricanes.

1. Introduction

As the popularity of coastal living increases and brings about a greater coastal population, both coastal property value and the potential of losses in these properties ascends as well. Though not the deadliest year on record, the recent 2017 hurricane season inflicted an estimated 300 billion US dollars of damages on the Eastern Seaboard of the United States, the highest in recorded history. 2018 culminated in another 50 billion US dollars of damage, headlined by Category 4 Hurricane Florence and Category 5 Hurricane Michael, the latter accounting for over half of the annual total. The Florida Panhandle, the location of landfall for Hurricane Michael, faced both catastrophic winds and accompanying storm surge. Considerable efforts have been made in the reduction of losses in the event of these hazards, both in the planning and response stages of a disaster. Among the structural mitigation planning for these coastal storms is the use of elevated buildings.

An elevated building is defined as one, where either portions of or in its entirety is situated above the ground on a structural system consisting of piers or stilts. Elevated buildings are most commonly used as a form of mitigation against potential flood hazards which may accompany storm events by means of heavy rainfall or coastal storm surge. In this case and as depicted in Fig. 1, the building *elevation*, defined as the distance between the ground plane and the underside of the building floor (sometimes measured to the lowest horizontal structural member or to the front door elevation), must be designed such that the structure remains above the expected stillwater elevation and wave heights for a given flooding intensity (commonly described using a return period). On the other hand, the building *height* is used to describe the distance between the ground to a particular point being considered (often the mean roof height) and is distinguished from *elevation* in this paper. In many jurisdictions where the construction of elevated homes is prevalent, a freeboard depth, e.g., the clear distance between the floodwater elevation and building floor, is also commonly mandated. For instance, in Florida, where storm surge was significant during Hurricane Michael, a freeboard depth of 1 ft is codified within the state building code and is of particular importance for residential

* Corresponding author.
E-mail addresses: j119k777@ku.edu (J.H. Kim), mmoravej@walkerconsultants.com (M. Moravej), enjsutley@ku.edu (E.J. Sutley), chowdhur@fiu.edu (A. Chowdhury), tndao@eng.ua.edu (T.N. Dao).

https://doi.org/10.1016/j.engstruct.2020.111101
Received 19 September 2019; Received in revised form 28 May 2020; Accepted 8 July 2020

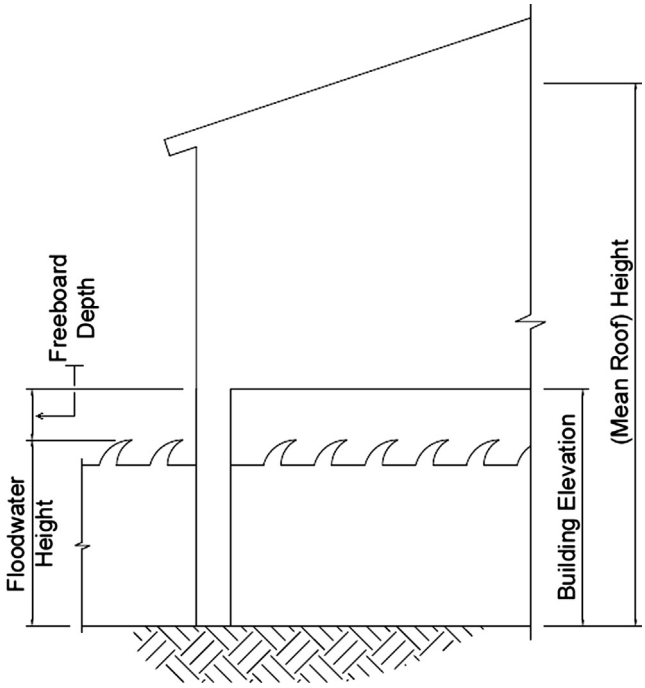

Fig. 1. Vertical measurements used for elevated buildings.

buildings in high flood risk zones (defined by the Federal Emergency Management Agency, FEMA).

Alternate building types exist that may also be classified as an elevated building. These include residential buildings constructed with an underlying crawlspace, as well as manufactured homes (also commonly known as "mobile homes") situated on steel chassis systems, or steel or concrete footers. Skirting is commonly attached around the perimeter of manufactured homes to, amongst other purposes, reduce the wind passage through the air gap. Unfortunately, skirting commonly becomes detached in high wind events (Fig. 2).

The aerodynamic effect of the air gap underneath the floor of elevated houses is not codified and thus neglected during design. As noted by Vann and McDonald [1], the presence of the floor underside pressures in manufactured homes may exacerbate the uplift of these structures in severe wind events. In some cases, the detachment of the structure from the ground may occur, causing a shift of the structure from its original position or even an overturning of the building. In contrast, buildings elevated higher are hypothesized to experience greater negative pressures (or suctions) on the underside of the floor; it

Fig. 2. Manufactured home situated on concrete block footers with damaged and partially-removed skirting, damaged in 2018 Hurricane Michael. (Photo credit: Josh Hunt, University of Alabama.)

is expected that a sufficiently-large air gap will induce higher magnitudes of negative pressures as on the roof, due to flow separation at edges and turbulent eddies. Uplift forces on the roof would thus be counteracted by these floor underside pressures which could reduce the overall uplift forces on the main wind force resisting system. Conversely, damages are expected to occur to the underside components and cladding, which can be removed by high wind suctions if not properly attached.

Limited amount of field data are available pertaining to the state of elevated residential buildings following a high wind event. Two sets of field data are noted for their inclusion of height of building elevation and related damage states: the first from a population impact survey in south Miami-Dade County, FL, following 1992 Hurricane Andrew [2], and the second from an assessment of damages due to 2008 Hurricane Ike in Galveston County, TX [3,4]. While correlations can be made in regard to the recorded damages and survivability of elevated homes, such empirical relationships are not sufficient for recommendations in structural analysis and design.

The majority of previous research concerning wind on elevated buildings has focused on manufactured housing, though even such research remains very limited, especially in regards to wind pressure measurements. Manufactured housing, which can be considered a subset of elevated buildings, was scrutinized for poor behavior in high wind events as far back as 1977, the year in which the U.S. Department of Housing and Urban Development (HUD) published the results of a six-month study of wind measurements on a full-scale manufactured home [5]. The HUD report detailed the wind loading on the entirety of the manufactured home specimen. However, results are limited due to the testing being performed on an outdoor set-up where the specimen was placed on a turntable in a parking area known to have heavy winds and the floor pressure was only measured at the centerline of the building and generalized over the entire floor area.

Later in 1983, Roy utilized an open circuit boundary layer wind tunnel to model the effects of wind loading on a 1:100 scale manufactured home model, in an effort to compare small-scale wind modeling results to full-scale field measurements [6]. Horizontal force coefficients were found to be greater on the full-scale model by up to 75%, thereby showing an underestimation of the wind forces on the structure by the wind tunnel procedure. This underestimation was attributed to a disparity in the effects of Reynolds number in the wake region. Closer results were obtained in the comparison of vertical force coefficients when skirting was present, with differences of only about 13%; however, this was not the case when the skirting was removed, where the recorded forces on the 1:100 scale model were as much as 28% smaller than in the full-scale case. Once the skirting was removed, the lack of modeling of the support underneath the structure was highlighted as a potential source of discrepancy.

Though manufactured homes could exhibit similar aerodynamic characteristics as conventional site-built elevated buildings, manufactured homes are not featured in this paper. Instead, focus is placed on the field observations of site-built homes purposefully elevated to reduce impacts from flooding and storm surge. Open circuit boundary-layer wind tunnel modeling on site-built elevated low-rise structures had also been conducted as well, albeit again for smaller scale models of 1:50 and 1:100 [7]. Notably, the 1994 study by Holmes included an elevated building case among other testing configurations, where the model house was elevated based on a full-scale height of 2.1 m (6.9 ft). Both the roof and wall mean pressure coefficients on the elevated structure were observed with greater magnitudes compared to non-elevated specimens, where mean pressure coefficients differed by as much as 50% on the roof and 100% on the walls when the wind direction was perpendicular to the roof ridge. Root-mean-square and peak pressure coefficients were also higher in the elevated case. An increase of mean wind speed at the eave's height of 20–30% greater translated to a potential pressure increase of 40–80%. However, no conclusions were offered regarding negative floor pressures, as this was not an objective

of their study.

There have also been studies regarding alternate interpretations of elevated structures. Liu et al. investigated the turbulence and eddy dynamics in pedestrian-level winds beneath larger, multi-story elevated buildings (referred to as being "lift-up") [8]. The term "elevated structures" was also used to refer to smaller additions to larger buildings, such as skylights and water storage tanks, for which a dynamic response analysis methodology for wind was developed [9]. Due to the size of the structures investigated, as well as their main research intentions, these studies provide no input for the case of one- or two-story residential homes.

Previous experimental testing involving roof pressure and velocity coefficients for varying mean roof heights had been conducted in the NHERI Wall of Wind (WOW) Experimental Facility (EF) located at Florida International University (FIU) using 1:20 scale models of low-rise buildings with a half-hip roof [10]. The intent of the study was to determine the possibility of using the results of roof pressure coefficients for one building height to estimate the roof pressures for a similar building with a different height. In this case, no air gap was simulated beneath the building models tested; instead, the change in building height was the result of increasing the number of stories of the building. The most relevant results of the study show that both peak pressure coefficients and velocity coefficients on the hip roof tested did not change considerably with increasing building height, with the exception of the coefficients in the corner of the roof which increased. However, the applicability of the roof pressure relationships are unknown for elevated buildings where an air gap exists beneath the structure. The analyses presented here examine changes in roof and exposed (underside) floor pressure coefficients as a function elevation and height.

Current design provisions do not have adequate guidance for the aerodynamic loading on an elevated building. In the United States, the American Society of Civil Engineers (ASCE) 7 Standard for Minimum Design Loads and Associated Criteria for Buildings and Other Structures [11] is widely-adopted as the legally-required wind load provisions for structural design. Chapters pertaining to the determination of wind loads on typical structures have been included since the first edition of this standard, ASCE 7-88 [12], and have evolved and expanded considerably to the most recent edition, ASCE 7-16, to include commentary for non-straight line winds (e.g., tornados) and rooftop photovoltaic panels, among others. However, no provisions exist in ASCE 7 pertaining to wind loading on elevated homes.

In 2011, FEMA published P-55, the Coastal Construction Manual, to be used for the design and construction of residential buildings in coastal areas [13]. Elevated building design and construction is outlined and recommended for those regions susceptible to storm surge. Structural design considerations include the load determination on residential buildings; in this manual, the wind load determination follows the provisions of ASCE 7-10. The design for the structure and its roof and wall components are described; however, floor underside wind loads are only briefly acknowledged in the manual. No recommendations for the determination of wind loads on the underside of the structure is provided.

The governing hypothesis leading this research is that the elevation of a building, resulting in an air gap beneath the building, will modify the building's aerodynamics and induce wind pressures on the building surfaces that are different from those for a similar building that is not elevated. Moreover, the airflow underneath the building will result in negative pressure (suction) on the exposed underside of the lowest floor. This research is timely given that floor underside cladding or structural failure due to a design that does not consider realistic aerodynamic pressures can result in considerable losses or injuries due to collapse or water infiltration.

This paper describes the effect that building elevation has on wind pressures using observations recorded from a field research study conducted in the Florida Panhandle following 2018 Hurricane Michael. This hurricane proved to be one of the largest challenges faced by the Gulf Coast region of the United States in the past several years, since the landfall of Category 3 Hurricane Dennis in 2005.

October 10 marked the landfall of Hurricane Michael near Mexico Beach, Florida. The National Hurricane Center classified this event as a Category 5 storm with estimated sustained wind speeds over water of 249 km/h (155 mph) and a minimum central pressure of 91.9 kPa (919 mbar).These intense conditions also brought about a 4.3 m (14 ft) storm surge at Mexico Beach; catastrophic damages to nearly every coastal building in Bay County, and left Mexico Beach devastated. Extensive damages reached to nearby coastal cities such as Panama City and Port St. Joe, and further inland. As Hurricane Michael moved northward, it entered southern Georgia as a Category 3 hurricane and eventually dissipated. A Major Disaster declaration was made by FEMA in five Floridian counties: Bay, Gulf, Wakulla, Franklin and Taylor Counties; the storm resulted in the deaths of 72 people, and at least 5.5 billion US dollars of insured losses in Florida alone.

2. Hurricane Michael field study

Ten days after the landfall of Hurricane Michael, a National Science Foundation-funded RAPID field research study was launched in the impacted areas of the Florida Panhandle. The overall goals of this study were the on-the-ground observation and classification of damages to elevated structures and manufactured homes as a result of the hurricane. Six researchers from the University of Kansas and the University of Alabama conducted this study from October 20 to 24, 2018. Much of the debris on the roadways were cleared at this point, allowing access into the affected areas. However, at the time of the study, the majority of Mexico Beach remained open only to residents and authorized disaster management personnel.

Upon arriving in Florida, the team first moved to use internet resources to identify potential locations with elevated structures, namely coastal regions near Panama City and Mexico Beach, the most populated areas in the proximity of the location of the hurricane's landfall. Google Satellite and Street View imagery was used to observe the general regions. Preliminary wind maps, showing estimated peak 3 s gust wind speeds at 10 m above ground over flat open terrain, from Applied Research Associates, Inc. (ARA) were used to inform this planning process. The winds in these maps were estimated by using the peak gust winds recorded at numerous wind stations, including local Florida Coastal Monitoring Program towers and the National Oceanic and Atmospheric Administration's National Data Buoy Centers and Automated Surface Observing Systems. Data points from multiple wind speed regions were desired to help observe the efficacy and performance of elevated structures in high wind.

Data collection was facilitated through ArcGIS's Survey123 app. Using a customized survey form constructed for this investigation, field investigators were able to use their smart phones to compile recorded observations, collected photos, and site geo-tags into a single data point. The customized survey included building attributes, such as elevation height and number of stories, as well as questions to document damaged components and classify damage states. A total of 69 elevated structures were surveyed in this study, located between Mexico Beach and Port. St Joe, Florida (geospatially depicted with ARA wind contours in Fig. 3). Considering the ARA wind maps, data points within three approximated wind speed contours of 193–209, 209–225, and 225–241 km/h (120–130, 130–140, and 140–150 mph) were collected. Note that these wind estimates pertain to an open terrain condition (approximately ASCE 7-16 Exposure Category C) instead of if they were flowing over open water (ASCE 7-16 Exposure Category D). However, adjustments to the wind speeds in terms of exposure and mean roof height were deemed unnecessary for the purposes of guiding in-field data collection.

Of the 69 elevated buildings surveyed, 50 were observed to have some form of floor underside cladding; for the remainder of the

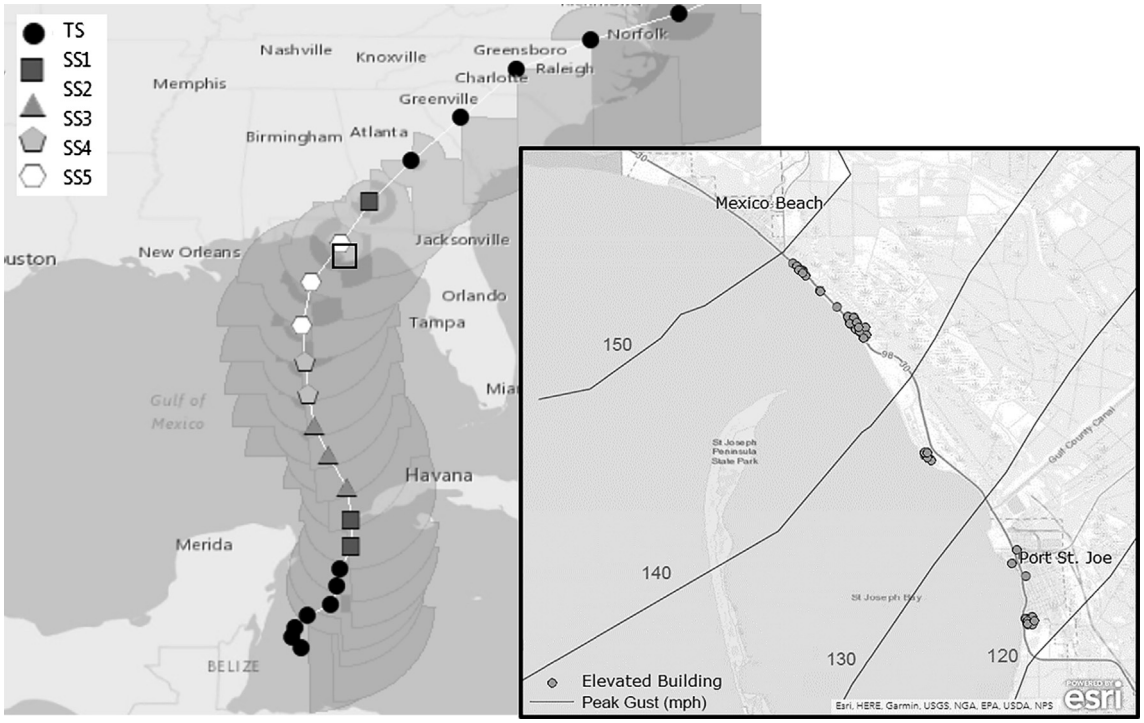

Fig. 3. Hurricane Michael best track and radii of hurricane and tropical force winds on Saffir-Simpson Hurricane Wind Scale (Data from [14]) with inset of location of elevated buildings surveyed following Hurricane Michael.

Fig. 4. Types of floor underside cladding and damage observed after Hurricane Michael; (a) vinyl with fastener failure, (b) hardboard with panel failure, and (c, d) wood structural panels with fastener failure. (Photo credits: (a, b) Elaina Sutley, University of Kansas, (c) Josh Hunt, University of Alabama, (d) Jae Kim, University of Kansas.)

buildings, it was unclear from the observation photos if cladding was present, or the sheathing panels on top of the floor joists were left exposed. These claddings generally consisted of either vinyl slats or panels, hardboard panels, or plywood or oriented strand board panels (see observed cladding examples in Fig. 4). Within the 50 cases with cladding, survey photos show that at least 28 were visibly damaged, with a minimum of detachment of some cladding from the supporting members. Detachment of vinyl cladding and fracture of hardboard were the most common forms of damage, with limited damages seen in the wood structural paneling. In addition to aesthetic concerns, damages

Table 1
Observations of floor underside cladding damage after Hurricane Michael.

ARA-estimated 3-sec gust wind speed at 10 m above ground	Number of elevated buildings surveyed	Number of elevated buildings with floor underside cladding	Number of floor underside claddings damaged
193–209 km/h	11	4	1
209–225 km/h	9	7	2
225–241 km/h	49	39	25

and removal of floor underside cladding can expose structural members and possibly lead to water infiltration into the building during or after the storm event.

As shown in Fig. 3, elevated buildings were surveyed across three levels of estimated peak wind speeds. Though many more elevated buildings were surveyed in the highest wind speed region (just southeast of Mexico Beach), a trend toward more cases of floor underside cladding damage at higher wind speeds is clearly identifiable. A summary of the cladding damage breakdown is presented in Table 1.

Basic post-storm analysis identified building cases which may have flooded during peak storm surge inundation depth. This analysis used the hindcast inundation models for Hurricane Michael published by Coastal Emergency Risks Assessment [15]. Inundation depths above ground were obtained for locations of each elevated building surveyed during the field study, and compared to the recorded elevation of the lowest horizontal structural element for each building. Only eight of the damaged cases were expected to have been partially underwater during storm surge flooding; another eight of the undamaged cladded cases were also expected to be inundated. Thus, a large percentage of the damaged cases are assumed to be the result of wind damage alone, rather than due to storm surge floodwater loading or a combination of the two. It should be noted that the time of maximum inundation depth is not necessarily expected to coincide with the occurrence of the maximum wind gusts; therefore, conclusions regarding wind pressures and damage at the time of significant storm surge were not made.

No clear correlation could be discerned between elevation height above grade and whether the floor underside cladding would be damaged or not. Unfortunately, accurate estimates of cladding damage were unable to be determined using the collected photos for the majority of the buildings surveyed. However, at least some evidence of damaged cladding due to wind was observed on buildings elevated in a range of 1.7–3.7 m (5.6–12.0 ft). A total of 57 of 69 buildings were elevated within this range encompassing the majority of the range of all building elevations observed during the field study (0.4–4.9 m; 1.3–16.0 ft).

The modes of failure observed consisted of both fastener failure and panel failure, though the former appeared to be more frequent and based on the regularity in shape of the cladding losses (loss of entire rectangular sections between connection locations). An example of each type of failure is provided in Fig. 4; the top photo shows the result of fastener failure where entire panels of cladding are removed, and failure of the panels themselves can be seen in Fig. 4b. The locations of floor underside cladding damage were often near the edges of the surveyed buildings (Fig. 5). Such a pattern would be consistent with locations of high pressures on wall or roof surfaces of a building, where flow separation occurs at edges. Additional damages were also seen closer to the center of the floor surfaces, where significant cladding panel loss was observed (Fig. 6). The damage to the central areas of the underside floor may be the result of progressive panel loss, initiating with fastener loss at the floor edges and leading to wind infiltration into the cavity between the panels and the structure. This panel loss over large areas may also be attributed to the simultaneous occurrence of high suctions; this phenomenon may occur due to high correlation of aerodynamic pressures across large sections of the floor underside. Such correlations were analyzed using wind tunnel test results and will be discussed in a later section.

Fig. 7 presents examples of damage patterns observed on three particular coastal homes residing between Mexico Beach and Port St. Joe. Building IDs are assigned to each home and are associated to the Object ID labels of the data points collected during the field survey [16]. The elevating structures, columns or poles, are shown in crossed squares or circles respectively. Dashed lines represent the location of elevated decking, under which floor underside cladding was typically not used. The properties of the three buildings from Fig. 7 are described in Table 2.

As seen in Fig. 7, much of the wood structural panel cladding did not remain intact in the presence of the 225–241 km/h (140–150 mph) 3-second wind gusts estimated by the ARA wind maps for this area, the highest speeds in the areas surveyed. A photo of the underside of Building 225 is presented in Fig. 8 in which both fastener failure, on the left, and panel failure, near the center, can be observed. Examples of the edge cladding failures and possible progressive inner cladding damage is observable in the damage location maps in Fig. 7.

3. Experimental testing

To supplement the empirical data obtained after Hurricane Michael for more specific conclusions on underside floor wind pressures and damage patterns, the results of a relevant experimental test were obtained and examined.

3.1. Wind tunnel testing

The physical model testing was conducted using the WOW EF. The WOW facility features a 12-fan open-jet wind tunnel capable of simulating winds and wind-driven rain attributable to hurricane conditions. The WOW EF has a 6.1 m (20-ft) wide by 4.3 m (14-ft) high open-jet testing section. Triangular spires and floor roughness elements are used to simulate turbulence and boundary layer characteristics. The size of the testing section allows for testing of large- and full-scale models. Large-scale models (e.g., 1:30 or larger for low-rise buildings) are expected to reduce scaling errors relating to geometrical details and Reynolds numbers that can arise from using smaller-scale models [17], as well as reveal finer details pertaining to low-rise structures which may be missed at smaller scales [18].

The spires and floor roughness elements were configured to simulate an open terrain exposure condition. The wind speed profile and turbulence characteristics, as a function of height above the ground, were measured through the use of a pitot-static rake with a series of Turbulent Flow Instrumentation Cobra Probes. For the purposes of the testing, the winds were generated using a 40% fan throttle. This fan throttle rate was used to avoid the exceedance of the measurement range of the pressure scanners installed on the building models. The wind speeds at heights corresponding to the mean roof heights of the test model are listed in Table 3. Fig. 9 shows the wind speed spectrum observed in the wind tunnel when testing the 1.08 m mean roof height model, compared to the von Karman spectrum. Normalized longitudinal wind speed and turbulence intensities in the Wall of Wind facility are presented in Fig. 10, compared to target ESDU profiles [19].

Aerodynamic testing was conducted on a scale model of a single-story low-rise residential building. The prototype (full-scale) case-study building had length (L) × width (W) × height (H) dimensions of

Fig. 5. Examples of edge and corner floor underside cladding damage. (Photo credit: Jae Kim, University of Kansas.)

8.76 × 6.40 × 3.81 m (28.75 × 21 × 12.5-ft), with a gable roof pitched at 4 on 12 (Fig. 11). Four levels of building elevation were considered, using 0, 0.61, 2.13, and 3.66 m (0, 2, 7, and 12-ft) stilt heights. These elevations correspond to a non-elevated building (baseline case), a manufactured home case (low elevation), the original elevation of the case study building (medium elevation), and a further-elevated case (high elevation), respectively. Using 1:5 scale, the test model was reduced to dimensions of 1.75 × 1.28 × 0.76 m (69 × 50.4 × 30-in), with corresponding stilt heights (building elevations) of 0, 0.12, 0.43, and 0.73 m (0, 4.8, 16.8, and 28.8-in). The scaled model, pictured in Fig. 12, was produced using a wooden frame constructed from 2 × 4 lumber stock, and 9-mm thick clear polycarbonate panels; 4 × 4 lumber stock was cut to length to construct the stilts. Soffit overhangs and numerous stilts were not simulated in the scaled-model for the purpose of simplicity, resulting in a single stilt located at each corner of the building. The resulting generic building shape should be relatable to a greater variety of buildings, though the need for alternative building test configurations are discussed later in this paper.

Wind pressures on each model were captured using 363 pressure taps located along each exterior surface including the roof, walls, and floor underside, allowing for the determination of aerodynamic pressure distributions on the building models, including localized cladding loads. The pressure taps were connected to a total of six Scanivalve ZOC33 pressure scanners using tubing lengths varying between 0.3 m and 1 m, based on the height of the models. Corrections were done for the tubing length effect using the method described by Irwin et al. [20]. A Scanivalve DSM4000 Digital Service Module recorded high-resolution pressure time-histories at a sampling rate of 520 Hz. The pressure data were low-pass filtered using a cut-off frequency of 200 Hz. The aerodynamic testing for different wind directions was accomplished by using the WOW turntable. The symmetry of the test model allowed for reducing the required range of wind directions as 0–90°. Intervals of 3°were used to simulate the number of wind directions considered for each case. Pressures for each wind direction for each building elevation case were recorded for 60 s. The wind velocity was captured at the mean roof height for each elevation case during a separate test excluding the presence of the building model. The mean roof height velocity was used as reference wind velocity to estimate the pressure coefficients for each model.

3.2. Analyses of peak pressure coefficients

A prior study conducted by Stathopoulos and Surry [21] demonstrated the limitations of conducting large-scale wind tunnel testing, in that turbulence integral scales are not properly simulated in relatively confined testing spaces. In these cases, the large-scale, low-frequency turbulence effects are not fully-realized, causing a relative over-abundance of high-frequency turbulence effects. These issues can be satisfactorily addressed by using methods such as the Partial Turbulence Simulation (PTS) method [22,23], by adequately modeling the high-frequency turbulence effects in the experimental wind tunnel testing and analytically incorporating the effects of the missing low-frequency gusts as though they are quasi-steady. Through the use of PTS, the calculation of peak positive and negative pressures is conducted with the full spectrum of appropriate turbulence in real atmospheric flows.

The full-scale turbulence intensities and integral length scales were obtained referring to document ESDU 85020, which describes turbulence characteristics in strong wind conditions [19]. A target full scale roughness of 0.08 m was utilized for these characteristics. Wind velocity data captured by the Cobra Probes yielded the integral length scales and mean velocities at the model scale. For every test configuration, a one-minute duration for the model-scale testing was used. The peak pressure coefficients (reported later) were estimated corresponding to full-scale duration of one hour in order to estimate statistically meaningful results. All wind and structural conditions used for PTS are summarized in Table 4.

For the benefit of the comparison analysis of the test results, the

Fig. 6. Examples of large sections of cladding panel loss on the floor underside. (Photo credit: Jae Kim, University of Kansas.)

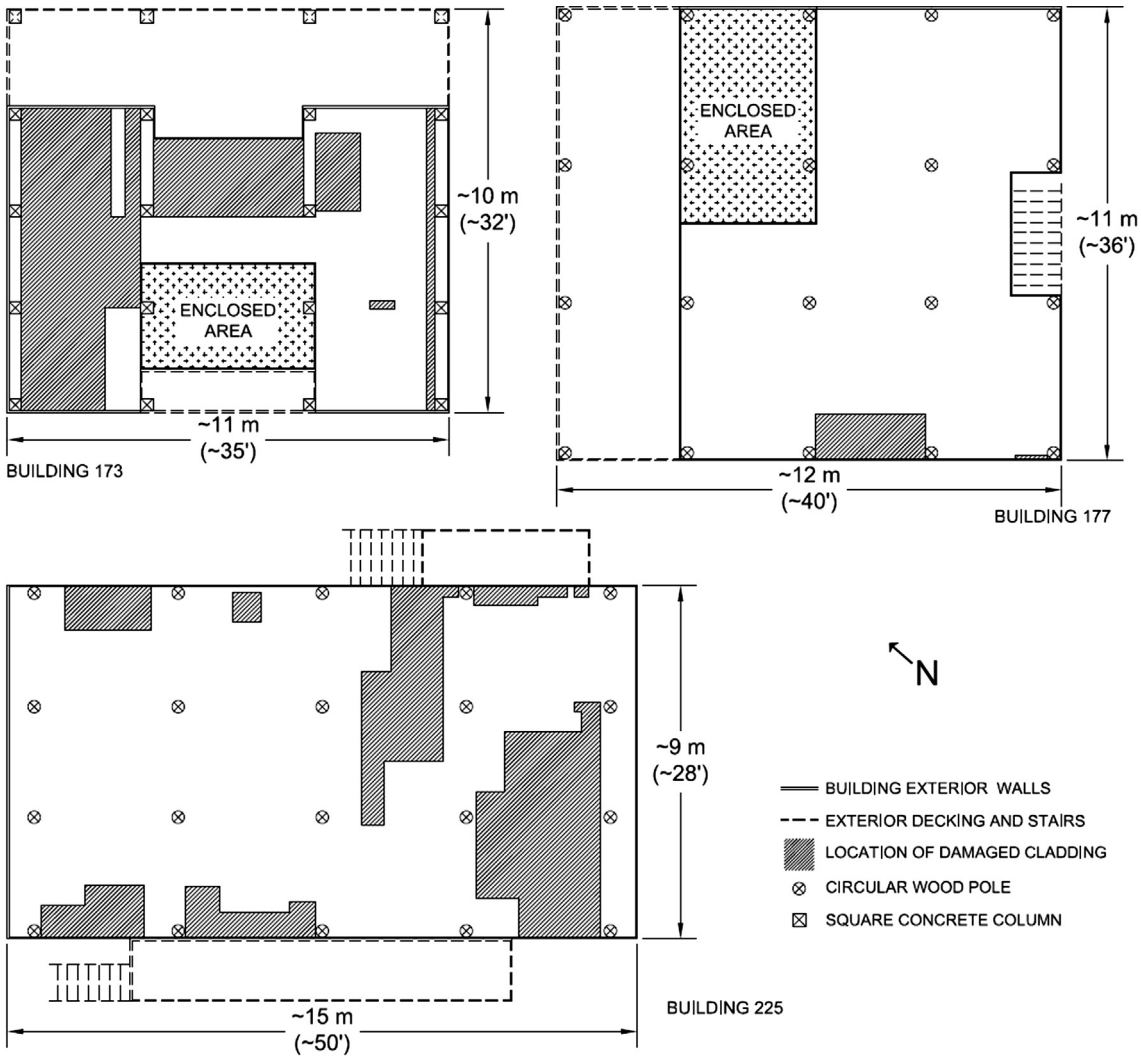

Fig. 7. Three examples of damage patterns (hatched) on floor underside cladding on buildings with ARA-estimated peak 3-second wind gust speeds of 225–241 km/h (140–150 mph).

recorded data was normalized into the form of pressure coefficients, C_P, by

$$C_p = \frac{\Delta P}{\frac{1}{2}\rho V^2} \tag{1}$$

where ΔP is the recorded differential wind pressure, ρ is the density of the air, and V is the reference mean wind velocity (at mean roof height of each model case). Peak pressure coefficients were obtained using the PTS methodology, the validation of which was described in Mooneghi et al. [22] and Moravej [23] based on comparisons of large-scale experimental results and field measurements on the Silsoe cube and Texas Tech University buildings. These coefficients can be used for the purposes of structural wind design, and are used in this paper for comparison of wind pressures on different building surfaces.

3.3. Pressure coefficient patterns

Linearly-interpolated contour maps of the peak pressure coefficients on the test model's roof and floor underside are presented in Figs. 13 and 14, respectively. These contours present the largest magnitude pressures on each region of the building surfaces, based on the worst aerodynamic pressures from the results of all the wind directions tested; negative (suction) pressure coefficients are shown, given that these pressures commonly have much higher magnitudes (and are mostly responsible for damage initiations) when compared to the positive pressures on these building surfaces. Only three contours appear in Fig. 14 due to the no elevation case not having an exposed floor surface to depict. Further, the large white sections in the bottom right corners of the contours in Fig. 14 are due to the supporting stilts and depict the locations where no pressure tap readings were taken.

Some clear trends can be seen within these results. First, the peak pressure coefficients on the roof surface do not noticeably differ with increasing building elevation. This is consistent with the results expected if the mean roof height of the building models were increased without the introduction of an air gap underneath, as demonstrated previously by Moravej et al. [10].

While no significant differences were observed in the peak pressure coefficients of the roof surface, the same cannot be said for the floor underside. Immediately obvious in Fig. 14 is the development of the higher peak pressure coefficients (in magnitude) approximately adjacent to the corner stilt at the higher elevation cases. At the 2.13 m and 3.66 m elevated cases, peak floor pressure coefficients reach magnitudes comparable to those on the roof corners and ridge, these being known critical locations for component and cladding pressures. Floor pressures coefficients were quite similar to each other for the 2.13 m and 3.66 m cases. Conversely, floor pressure coefficients greatly varied between the 0.61 m case and the two higher elevated cases. Looking closer at Fig. 14, high pressure coefficients are concentrated on the

Table 2
Example elevated building characteristics.

Building ID	Elevation	Elevating structure	ARA-estimated 3-sec wind gust speed at 10 m above ground	Floor cladding type, estimated percent failure
173	3.4 m (11.0 ft)	305 mm (12 in.) square concrete columns	225–241 km/h (140–150 mph)	Vinyl panels, 48%
177	3.2 m (10.5 ft)	305 mm (12 in.) diameter wood poles	225–241 km/h (140–150 mph)	Vinyl panels, 4%
225	2.4 m (7.9 ft)	254 mm (10 in.) diameter wood poles	225–241 km/h (140–150 mph)	Wood structural panels, 23%

Fig. 8. Floor underside cladding damage on the southeastern edge of Building 225. (Photo credit: Josh Hunt, University of Alabama.)

Table 3
Mean wind velocities at various heights above test floor.

Height above floor [m]	Mean velocity [m/s]
0.65	20.01
0.78	20.63
1.08	22.69
1.39	23.07

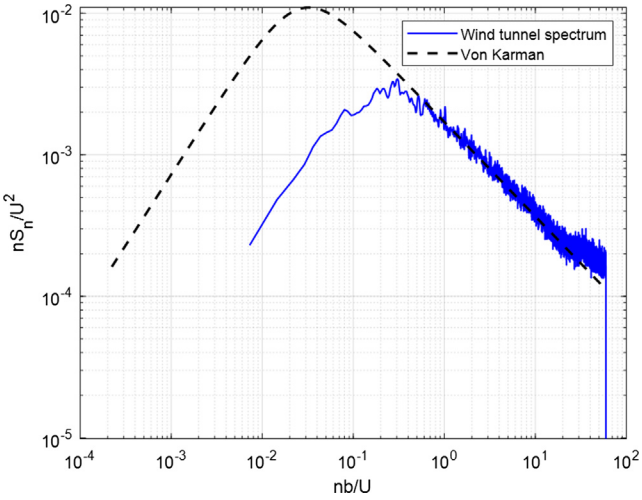

Fig. 9. Wind speed spectrum in the wind tunnel when testing the 1.08 m mean roof height model, compared to the von Karman spectrum.

windward edges, bounded by a sharp gradient in pressure coefficients; this suggests zones, such as those which are assigned wind pressure coefficients in ASCE 7, could be appropriate for floor underside wind pressure determination in codes and specifications. These locations of high pressure coefficient concentrations are compared to the field study observations at the end of the paper. Overall, the contours in Figs. 13 and 14 show that the pressure coefficients observable on the floor underside can be as concerning as those on the roof. The identification of the location of these critical pressure coefficients on the floor underside was also enlightening since this is necessary for design and can also be compared with observations taken from the field.

To take a closer look at the relative magnitudes of the roof pressure coefficients in comparison to those on the floor surface, cross-sections along the two horizontal dimensions of the floor and roof surfaces are taken. Fig. 15 provides the pressure coefficients along the horizontal length of the building at three cross-sections. Fig. 16 provides the pressure coefficients along the horizontal width of the building at three similar cross-sections. Distances along the length and width, respectively, were normalized with respect to the building dimensions. The

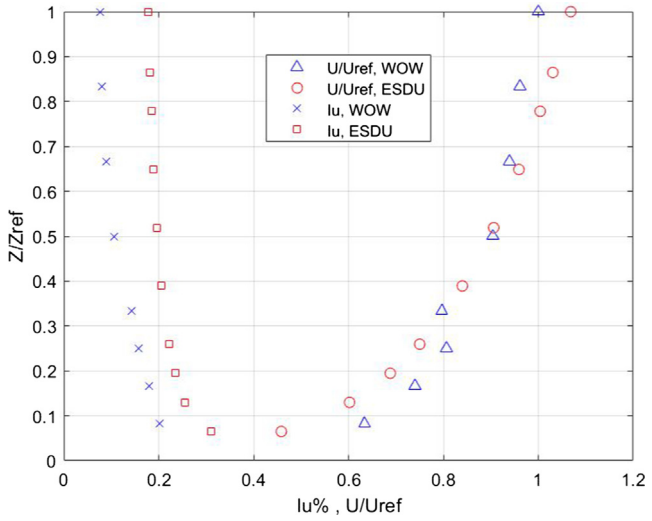

Fig. 10. Normalized longitudinal wind speed (U/U_{ref}) and longitudinal turbulence intensity (I_u%) in the Wall of Wind facility, compared to ESDU target profiles.

three cross-sections are taken along the midline, the edge, and at a section in between the midline and the edge, as denoted in the maps below the nine plots in Figs. 15 and 16.

In general, the magnitudes of the floor pressure coefficients were usually equal or lower than those of the roof across the entire building. An exception is noted in Fig. 15(e) and (h), where very large negative peak pressure coefficients occur adjacent to the stilts and at the edge of the floor underside. Similarly in Fig. 16(e) and (h), peak pressure coefficients on the floor exceed those on the roof near the edge. Much higher roof pressure coefficients are also observed along the roof ridge/floor underside midline (Fig. 15(a), (d), and (g)), where flow separation is possible on the roof but not on the floor. Similarly, much higher roof pressures are also observed along the roof ridge in Fig. 16 in all cross-sections and elevated cases. Notably in Fig. 15(c), (f), and (i), high peak pressure coefficients are observed on the roof near the corner, but cannot be compared to the floor since measurements were not possible at the stilts. This is similarly observed in Fig. 16(a), (d), and (g), where high peak pressure coefficients are observed on the roof near the corner, but not captured for the floor.

Another important observation was the distinction in the results due to the effect of building elevation on the wind pressure patterns, or lack thereof. Predictably, the change in building elevation did not greatly affect the magnitudes or patterns of the roof pressure coefficients. Indeed, the critical wind pressure coefficients on the roof did not vary significantly with increasing elevation, contrary to the findings of Holmes [7]; these results fall more in-line with those presented by Moravej et al. [10]. The overall wind pressure coefficient patterns on the floor underside were also quite similar for the two higher-elevated cases and less similar to the low elevation case. This trend is observable with both the contour maps as well as the cross-sectional plots. A possible reason for such a distinction is that the 0.61 m (full-scale) air gap beneath the building was small enough to significantly constrain the wind flow with the presence of the vertical stilts, the ground, and the floor underside surface. For those models with greater elevations, the increase in gap size between the underlying ground and the floor underside resulted in a wind flow which was not substantially constrained. In other words, the air beneath the 2.13 m and 3.66 m cases was able to behave more similarly to the relatively unconstrained air layer above the roof, while this was not the case for the 0.61 m elevated case. This hypothesis is revisited in the next section, where trends of pressure time-history correlation coefficients are investigated. The relative size of the stilts (approximately 0.44 × 0.44 m at full scale) should be noted here, as they create large, blunt bodies that disturb the wind flow and can result in the turbulent eddy formation.

3.4. Correlation coefficients

Cross-covariances pertain to signals at different points (therefore, separated by a non-zero distance) as well as at different times, separated by time intervals τ. The cross-covariance function of two stationary signals $z_1(t)$ and $z_2(t)$ with zero means, in this case fluctuations of the pressure time-histories at two pressure taps, is defined as follows:

$$R_{z_1 z_2}(\tau) = \lim_{T\to\infty} \frac{1}{T} \int_{-T/2}^{T/2} z_1(t) z_2(t+\tau) dt \tag{2}$$

The more z_1 differs from z_2,the lower is the value of the cross-covariance $R_{z_1 z_2}$. The cross-correlation coefficient of two fluctuating pressure signals is defined by the ratio of their cross-covariance by the product of their standard deviations, i.e.,

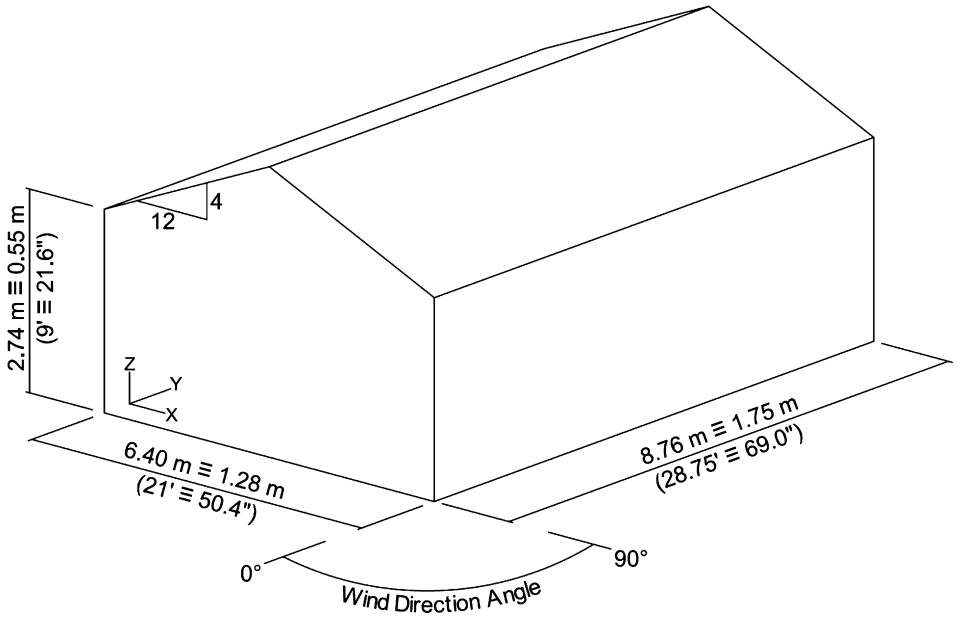

Fig. 11. Experimental test model dimensions at full-scale (1:1) ≡ large-scale (1:5), and wind direction orientations.

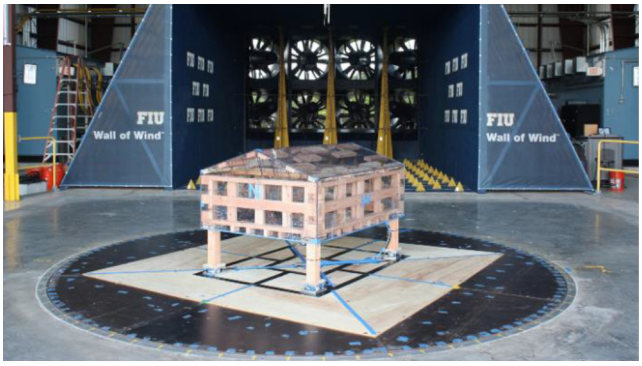

Fig. 12. Photograph of the elevated building test specimen, located in front of the wind tunnel spires and floor roughness elements. (Photo credit: Arindam Gan Chowdhury, Florida International University.)

$$\rho(z_1, z_2, \tau) = \frac{R_{z_1 z_2}(\tau)}{\sigma_{z_1}\sigma_{z_2}} \tag{3}$$

where σ_{z1} and σ_{z2} are the standard deviation of z_1 and z_2, respectively.

In this study, peak pressure coefficient estimations were supplemented with cross-correlation coefficients (for $\tau = 0$). Whereas the peak pressure coefficients are particularly useful in identifying critical pressure zones on the building surfaces, correlation coefficients of pressure fluctuations can provide information about the correlation of pressure signals (the extent to which they are in phase or out of phase) over effective wind areas to help articulate how area averaged pressure coefficients reduce as a function of increasing tributary areas. Note that, however, the correlation coefficients determined are not fully sufficient to develop wind pressure coefficient zones, as they are not indicative of the magnitudes of the pressure coefficients.

Cross-correlation coefficients of pressure fluctuations at taps on both the roof and floor underside surfaces were investigated and evaluated for three wind directions (0°, 45° and 90°) corresponding to wind traveling parallel and perpendicular to the gable roof ridge, and 45° between these two directions. The same six cross-sections used for the peak pressure coefficients and the three levels of building elevation were used when investigating the cross-correlation coefficients.

Correlations were determined at each cross-section by comparing the pressure time-history of the 'edge-most' tap (the pressure tap located closest to the building edge in the cross-section) with those of the taps of increasing distance along the cross-section. Therefore, correlation coefficients for increasing distances between measurement locations were obtained. The results are plotted in Figs. 17 through 22.

Larger correlation coefficients between pressure tap readings imply that the pressures are more correlated. Correlation coefficients close to unity are expected between pressure taps which are immediately adjacent to one-another, since the effects of the wind within a very small area should be relatively consistent. As the distance between pressure taps increases, this correlation is expected to reduce, implying that the peak wind loads at those locations do not occur simultaneously. Looking across Figs. 17–22, this behavior is observed consistently: the correlation coefficient is one at the far-left end of each subplot where the distance between points is zero and the correlation coefficient decreases as distance increases.

However, there are noticeable differences between how correlation coefficients change over distance for each of the roof and floor surfaces, cross-section locations, wind directions, and building elevations. Each of these are discussed individually. First, as seen across all cross-sections and wind directions, roof pressure correlations do not appreciably change as building elevation increases. The same cannot be said of the floor underside pressure correlations. For floor pressure correlations, higher correlation coefficients are generally observed at the lowest elevated case in comparison to the moderate and highest elevations. Similar to the contours and peak pressure coefficient cross-sections, differences between correlation coefficients for the moderate and higher elevated case on the floor are miniscule. The differences between the lower elevated case (2.13 m) versus the other two elevated cases is more pronounced in the horizontal length cross-sections at 0 and 45°, (Figs. 17(a) and 19(a)) and in the horizontal width cross-sections at 45 and 90° (Figs. 20(a) and 22(a)). It can be said that a more-constrained air flow beneath the building results in stronger correlations over larger distances, and at some point (in this case, at 2.13 m elevation) the air flow beneath the building is no longer meaningfully constrained. This is a critical observation, as the implication stands that buildings elevated to lower levels may have a higher propensity to experience relatively higher (in magnitude) area averaged negative pressures (suction) over large areas simultaneously, compared to those elevated higher off the ground.

Wind directionality also appeared to affect the correlations between tap pressures. In general, most roof and some floor pressure correlations tended towards zero more slowly when the cross-section was perpendicular to the wind direction. However, less subtle differences became apparent for a particular set of correlation coefficients along a cross-section; take for instance subplots (e, h) of Figs. 18, 20 and 22. Contrary to the other cross-sections investigated, a change in wind direction instead resulted in a flip in the concavity of the correlation coefficients decay over distance.

The cross-section location at which correlations were computed also influenced the behavior of correlation decay over distance. The most significant differences came between the floor cross-sections located along the edge of the building and those located closer to the middle. The influence of this cross-section position was less consistent: correlations along cross-sections parallel to the roof ridge were typically higher for the edges, whilst the opposite was true when the cross-section direction was perpendicular. In addition, this was less so the case for the roof, where for the most part, the shape of the plotted correlation coefficients appeared similar across-section locations.

Finally, general comparisons between roof and floor correlation coefficients were also made. Overall, the floor pressures showed either the same or higher correlations over larger distances than on the roof, especially for the 0.61 m elevated case, the clearest exceptions being the edge cross-section perpendicular to the roof ridge (Figs. 18 and 20(a), (d), and (g)). As stated earlier in this paper, the floor correlations at this low elevation were typically higher than for the higher elevations, whereas the roof correlations did not change noticeably with increasing building elevation.

Table 4
Wind and structural conditions used for PTS.

Stilt height [m]	Length scale	Turbulence intensity [%]	Integral length scale [m]	Mean velocity [m/s]	Duration [min]
0.61 (1:1) ≡ 0.12 (1:5)	Full scale (1:1)	21.24	22.65	46.59	60
	Model scale (1:5)	15.06	0.5	20.63	1
2.13 (1:1) ≡ 0.43 (1:5)	Full scale (1:1)	20.12	34.64	48.24	60
	Model scale (1:5)	10.54	0.5	22.69	1
3.66 (1:1) ≡ 0.73 (1:5)	Full scale (1:1)	19.35	47.45	49.52	60
	Model scale (1:5)	8.74	0.5	23.07	1

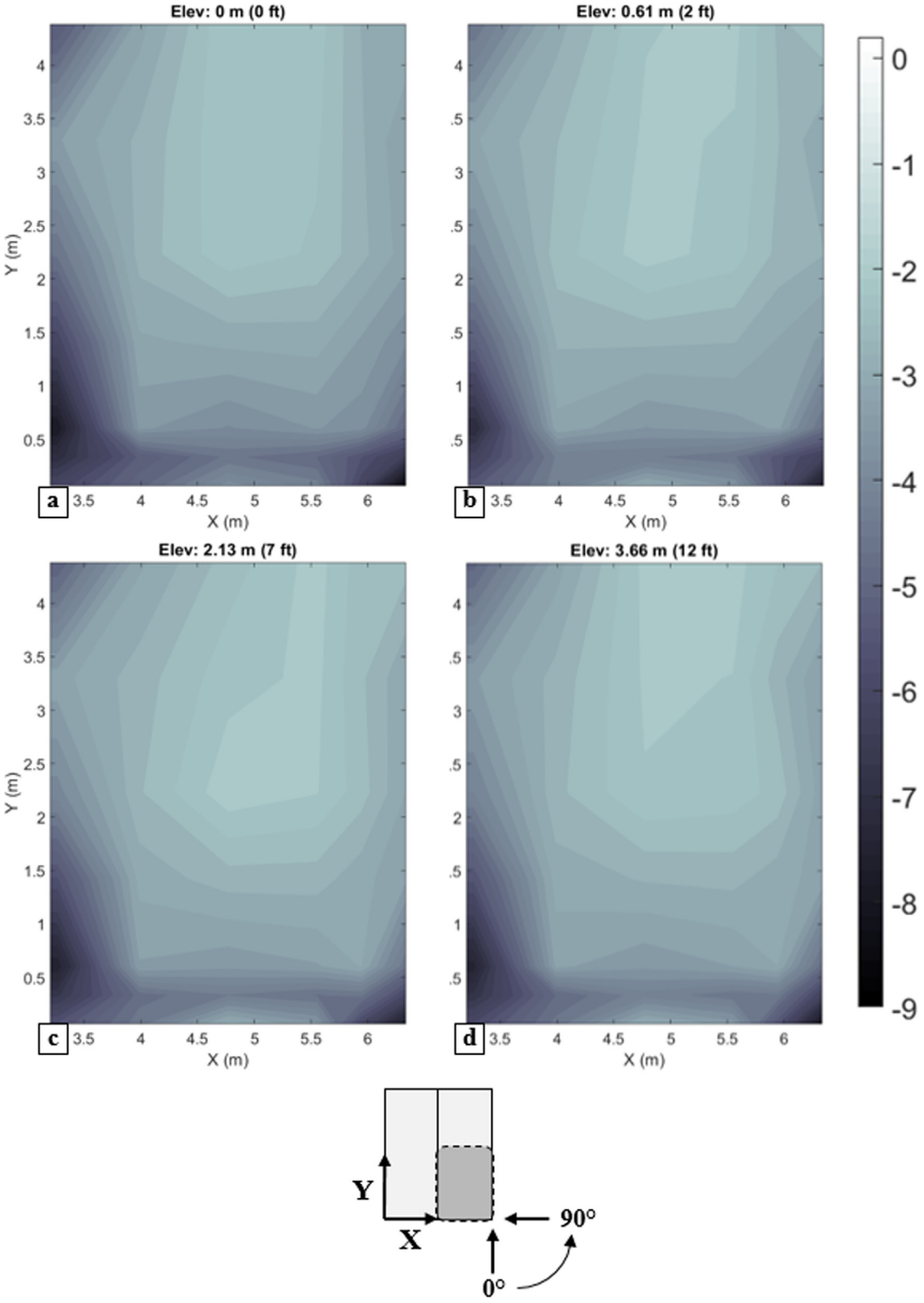

Fig. 13. Maximum (in magnitude) negative peak 3-second wind pressure coefficients on southwest gable roof for all wind directions: (a) 0 m, (b) 0.61 m, (c) 2.13 m, and (d) 3.66 m elevations.

4. Discussion

Both the observations from the Florida Panhandle and the wind tunnel testing show that floor underside pressures can be critically high, leading to damages to the building and its components. Improperly estimated pressures and subsequent design of components and fasteners can lead to avoidable losses in the midst of severe wind events. As demonstrated here, floor underside negative pressure coefficients can reach the same magnitudes as those on a gable roof, thus a deliberate design is necessary to limit damages. Fasteners at the edges of the

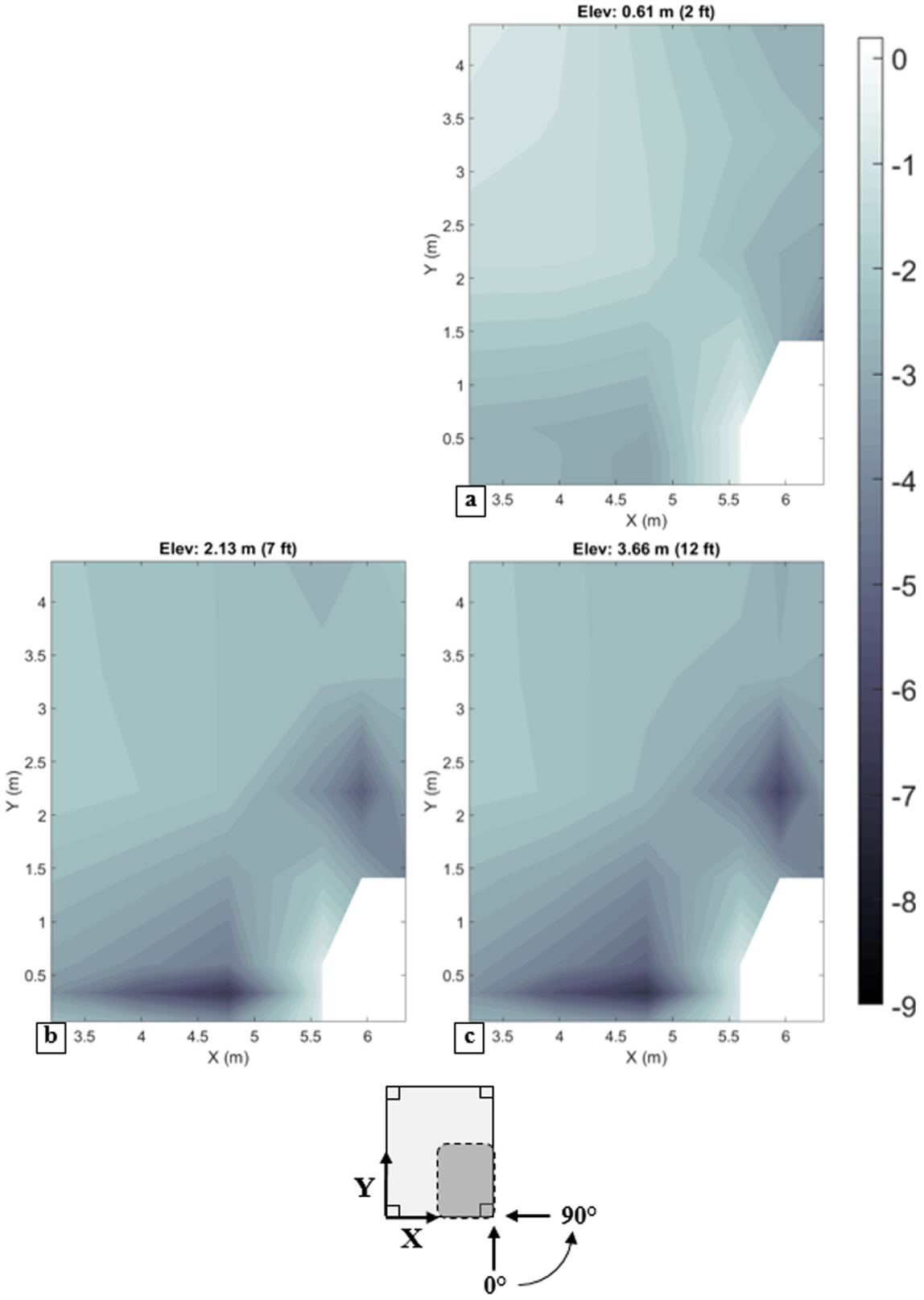

Fig. 14. Maximum (in magnitude) negative peak 3-second wind pressure coefficients on southwest floor underside for all wind directions: (a) 0.61 m, (b) 2.13 m, and (c) 3.66 m elevations.

building floor are of particular concern, where pressure coefficients are highest.

The positive pressure coefficients on the floor underside estimated from the wind tunnel testing were quite low and were disregarded in this study. While further experimental testing can discern more detailed conclusions regarding positive pressures, the effect of positive pressures on the building as a whole (for instance, if one considered uplift of the building) would appear to be minimal. Instead, it is the negative

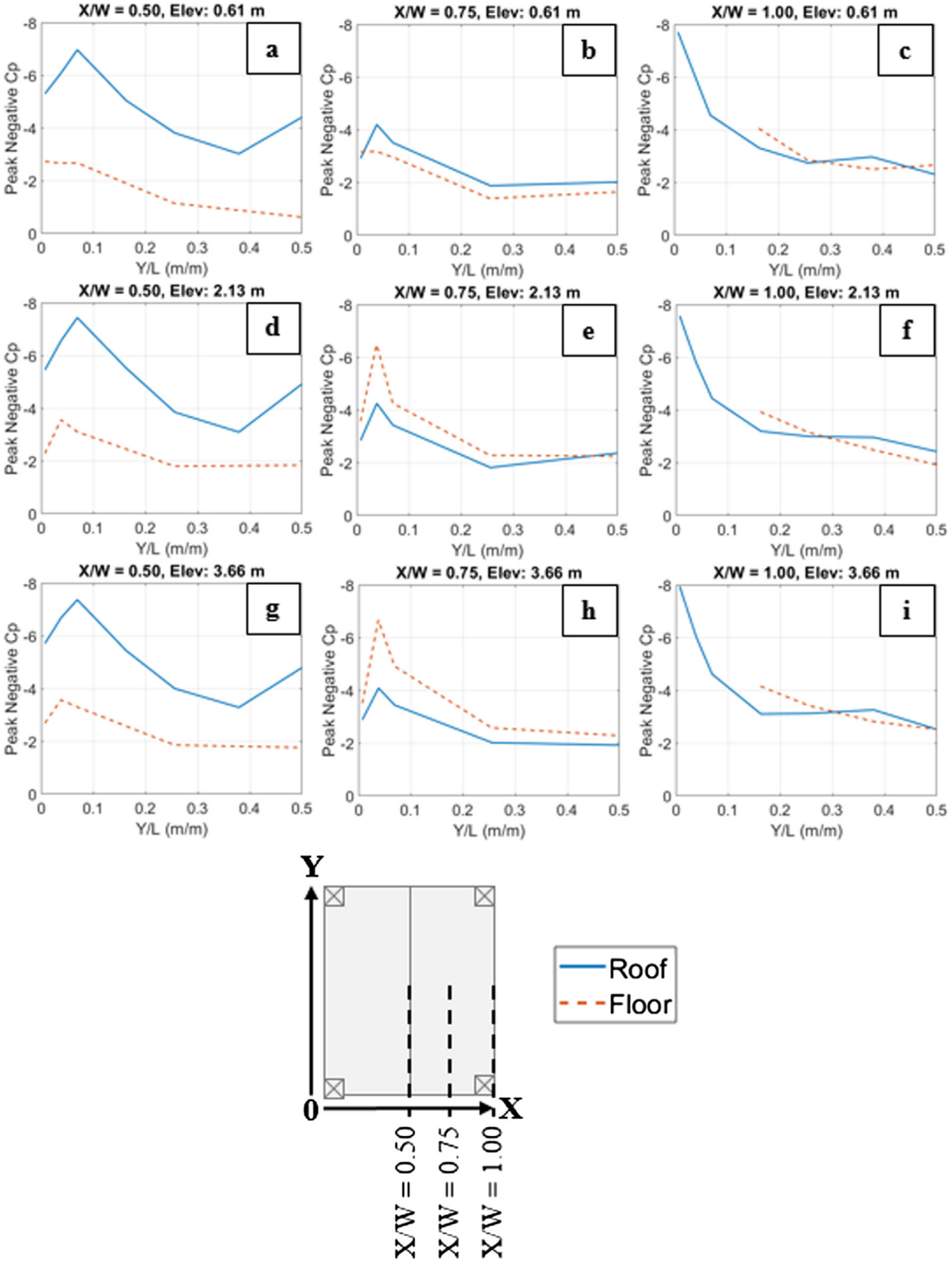

Fig. 15. Comparing the roof and floor maximum peak negative pressure coefficients (considering all wind directions) along a horizontal length cross-section of the test model. Each column and row refer to a cross-section location and a level of elevation, respectively.

pressures on the cladding and floor structural system which will warrant further investigation to inform proper design procedures for elevated buildings.

4.1. Connecting experimental work with Hurricane Michael survey

During the discussion of the field observations taken following Hurricane Michael, two patterns of wind damage to the floor underside claddings of elevated buildings were discerned, as demonstrated in Figs. 5 and 6: edge panel loss at the boundaries of the building floor, and widespread panel loss across the floor surface. These patterns are especially interesting due to the conclusions formed as a result of the experimental program conducted at the WOW. The potential for edge cladding loss is corroborated by the pressure coefficient patterns seen on the floor underside at higher elevations (Fig. 14), where there exists peak pressure coefficients comparable to those specified for gable roof

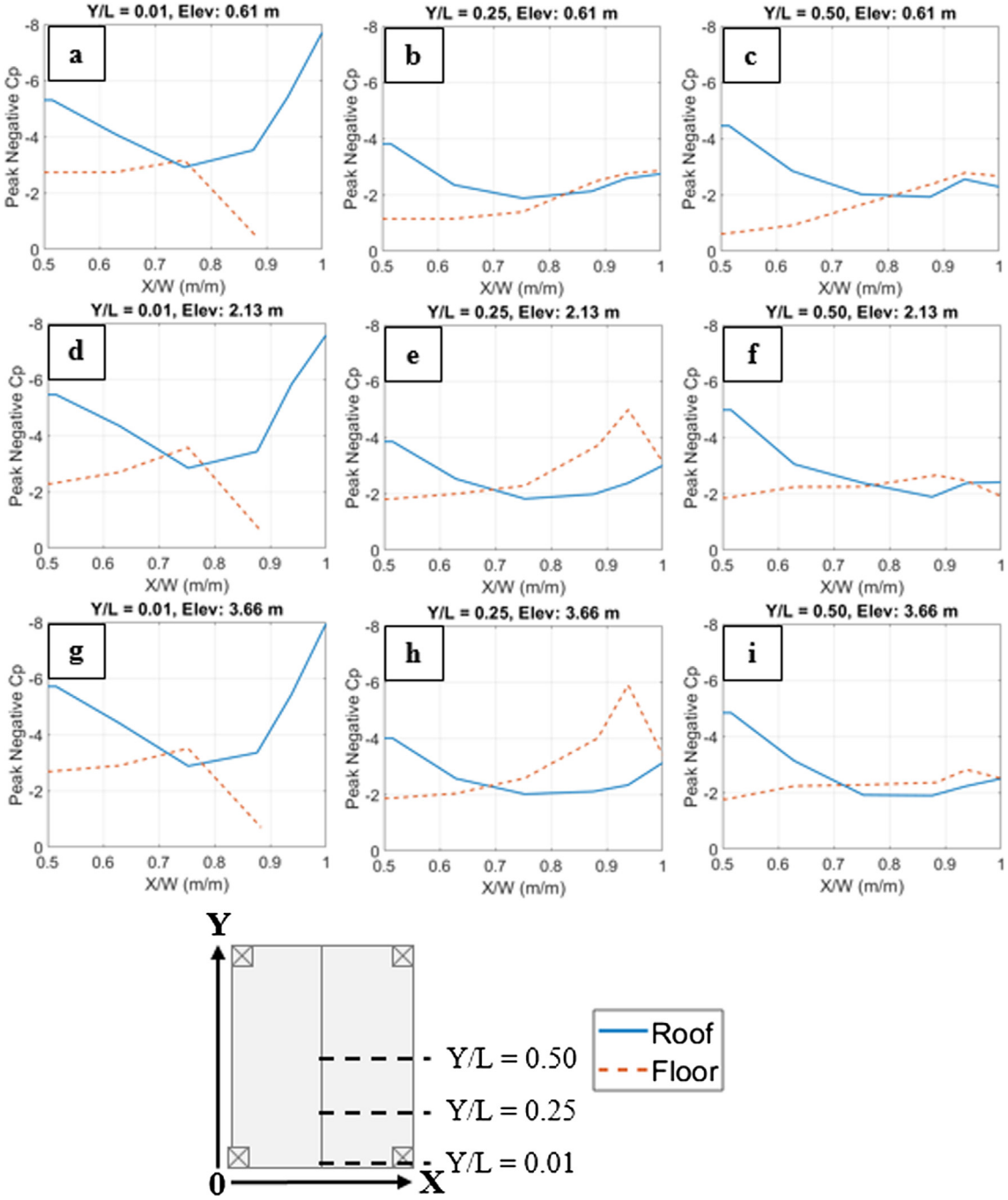

Fig. 16. Comparing the roof and floor maximum peak negative pressure coefficients (considering all wind directions) along a horizontal width cross-section of the test model. Each column and row refer to a cross-section location and a level of elevation, respectively.

component and cladding loads in ASCE 7-16. Damages to roof components (such as shingles and sheathing) are already regularly seen in the aftermath of severe wind events; corresponding damage to the floor underside due to similar potential of pressure loading should thus be expected and was observed for both roof and floor surfaces after Hurricane Michael. Note, however, that the structure tested at the WOW was highly simplified and lacks many building characteristics such as porches, overhangs and additional stilts which were seen on real-world homes. The results of the experimental testing are therefore not affected by these surface irregularities which would likely have resulted in different flow separation characteristics and consequently altered pressure patterns.

As noted in the analysis of the correlation coefficients study, the potential for high pressures acting over large areas of the floor underside also exists. It is ultimately not clear what the mechanism of damage was when large areas of the floor underside cladding failed in the field; it is possible that the damage occurred progressively or initiated via debris impact. The possibility of mass panel failure has been corroborated with the relatively high trends observed in the floor pressure correlation coefficients, and therefore remains a potential failure mode for elevated buildings.

Both such modes of floor underside cladding failure have ultimately been evidenced in the floor damage maps produced from the field case studies (Fig. 7). All three buildings portrayed in these damage maps experienced at least some edge cladding loss, and ample cladding loss for two of the cases. It is also important to point out that the wind

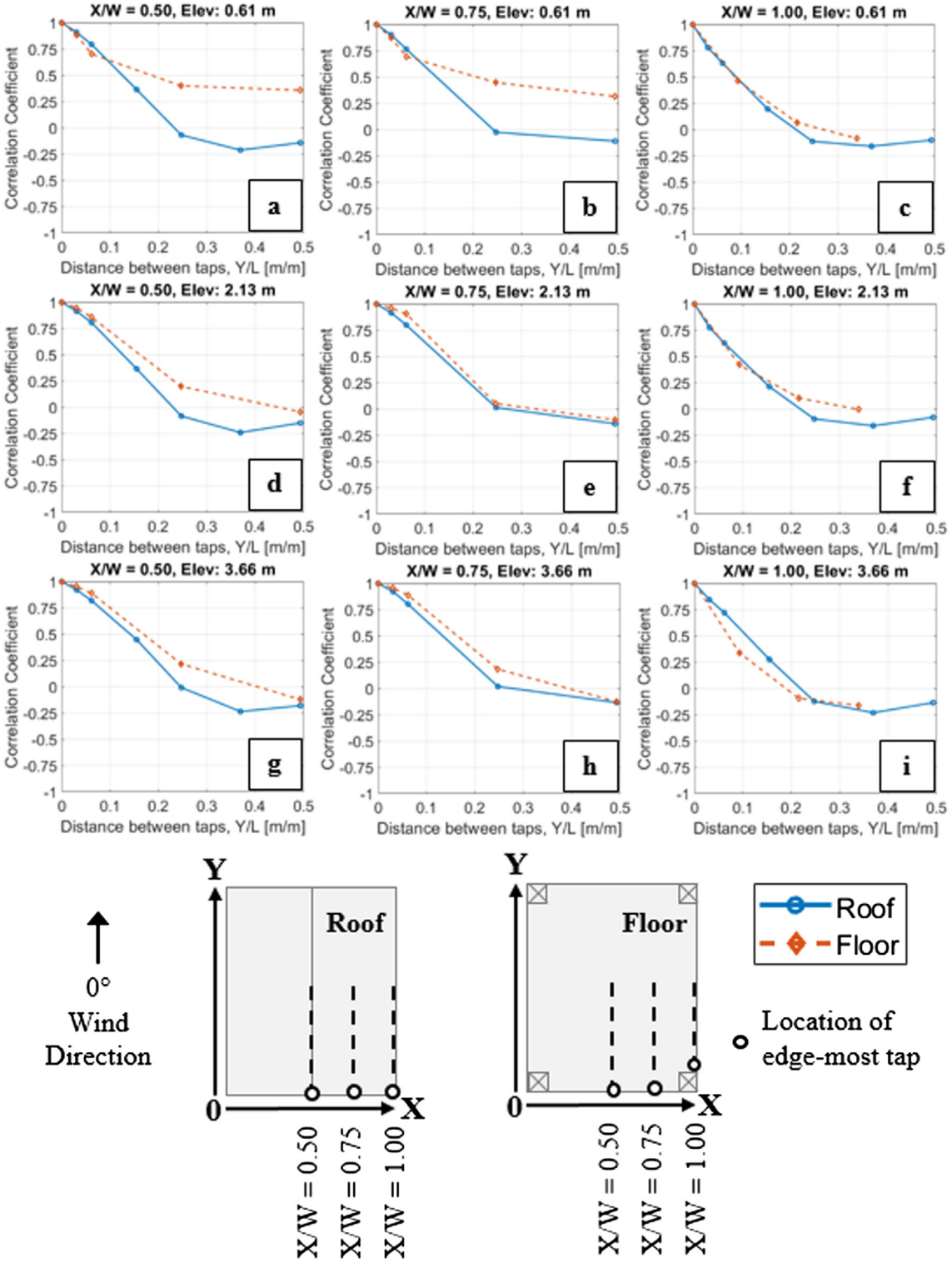

Fig. 17. Correlation coefficients between the edge-most tap and taps at increasing distances along a horizontal length cross-section, where both taps exist on either the roof or floor of the model, for a wind direction parallel to roof ridge.

tunnel testing was performed over a simulated open terrain exposure condition whereas the buildings observed in the field following Hurricane Michael were located in Exposure D denoted as flat terrain near the shoreline. These differences are not presumed to sacrifice the merits of the comparison provided here but should be considered in future studies.

The most susceptible elevated buildings will be those with relatively high pressure coefficients and higher correlations of pressures across the floor surfaces. The 0.61 m building had the highest correlation coefficients, but the magnitudes of the pressure coefficients were low enough to not necessarily cause damage. The 3.66 m elevated case will have damage at the edges due to very high suction, but may not have damage near the center as the correlation reduces quickly such that the area-averaged pressures over large areas are small. The 2.13 m elevated case will have edge damages, which may also extend to the center panels.

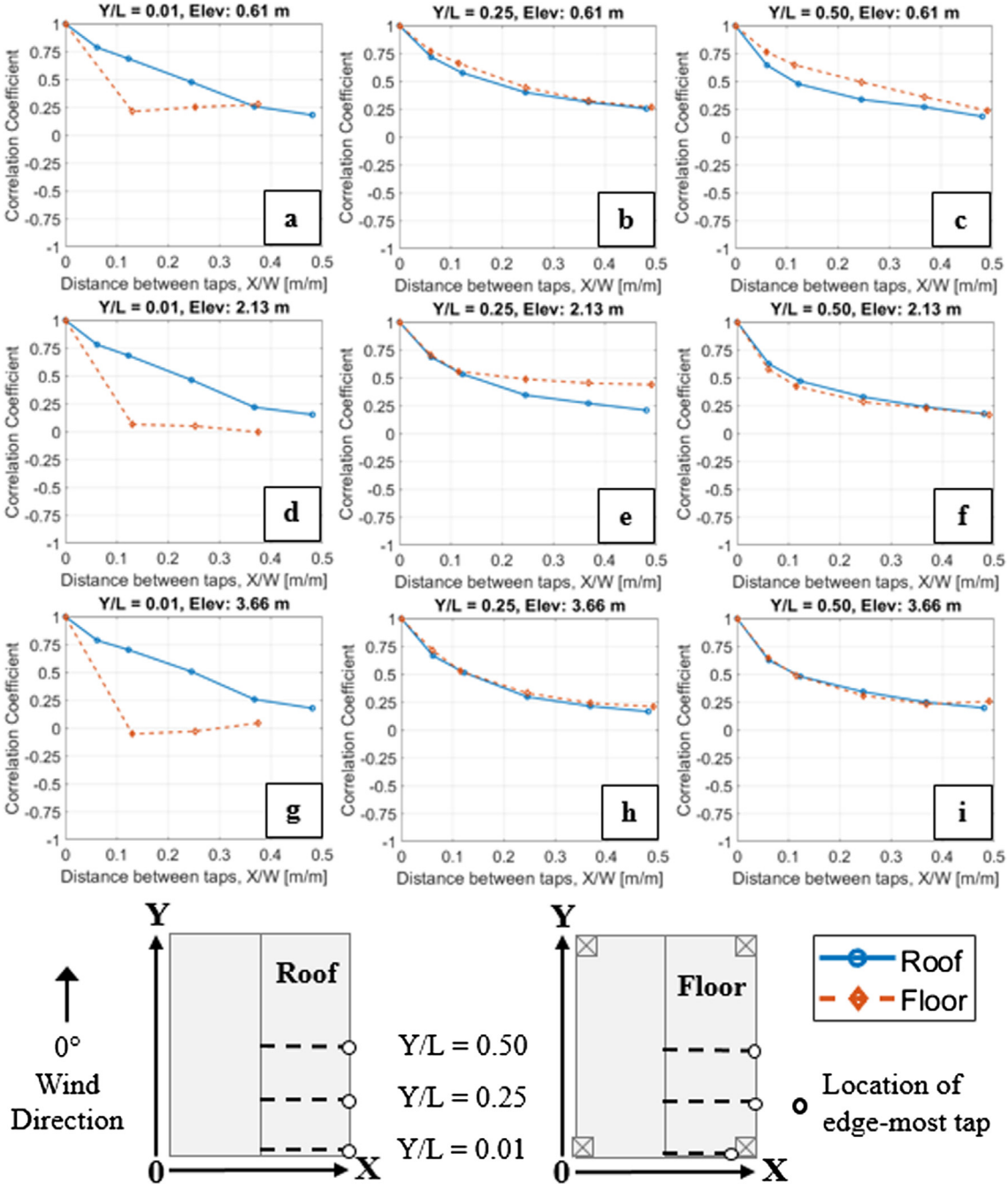

Fig. 18. Correlation coefficients between the edge-most tap and taps at increasing distances along a horizontal width cross-section, where both taps exist on either the roof or floor of the model, for a wind direction parallel to roof ridge.

Looking at Figs. 21 and 22, the correlation is maintained over long distances for the floor underside as compared to similar distances for roof surfaces. This means that area-averaged pressure coefficients will be relatively larger for floor underside surfaces compared to roof surfaces. The rapid change observed in ASCE 7-16 plots of pressure coefficients versus effective areas for roof component and cladding loads will be less drastic for floor underside component and cladding loads. More research is needed on area-averaged pressure coefficients for the floor underside. Nevertheless, these higher correlations could be responsible for damage propagation leading to progressive failures of large panels as observed in the field.

4.2. Potential for future research

The body of knowledge pertaining to wind pressures on elevated buildings will greatly benefit from further wind tunnel testing on large-scale models of differing building configurations with the goal of gaining insight into the aerodynamics of the elevated building. The testing conducted for this project has been limited to one building configuration of three heights above elevation, building aspect ratio, and gable roof angle. Compelling variables to test include the size and distribution of stilts, given their propensity to generate large negative pressures, and a finer distribution of building elevations to investigate the constriction of the underfloor air flow.

Likewise, further careful study of elevated homes and other buildings damaged during high wind events will also augment the

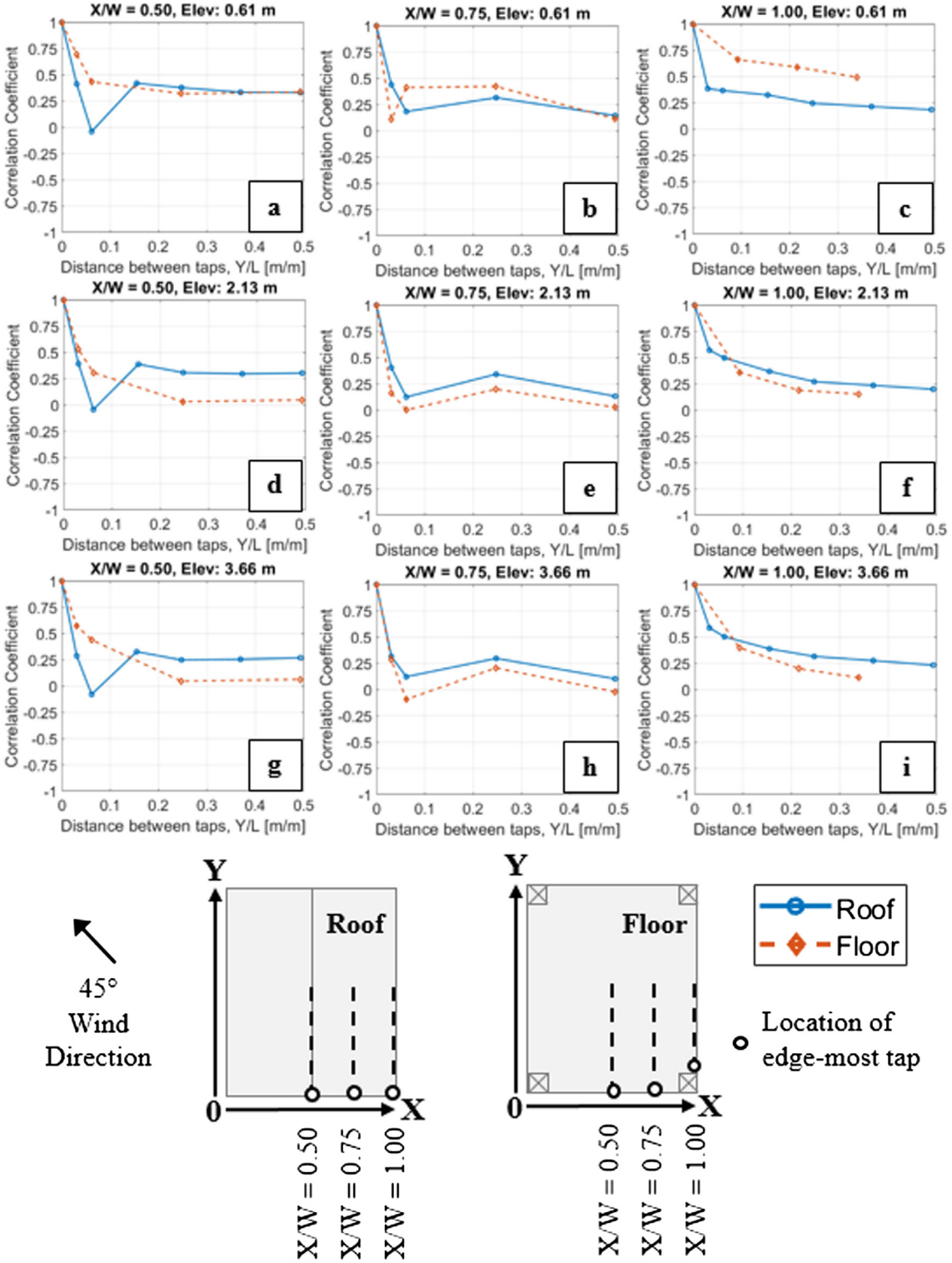

Fig. 19. Correlation coefficients between the edge-most tap and taps at increasing distances along a horizontal length cross-section, where both taps exist on either the roof or floor of the model, for a wind direction 45° to roof ridge.

understanding of wind pressure patterns on the vulnerable floor. Evidence of this sort of damage has already been presented in this paper; further refined findings are needed for robust design guidelines.

5. Conclusion

Given the observed lack of understanding of the wind aerodynamics and pressure distributions on buildings elevated above the ground, large-scale experimental wind tunnel testing and a field study following a major hurricane in the Florida Panhandle were conducted. Both studies were intended to produce preliminary observations regarding the wind pressures on the roof and floor underside of the building.

Floor underside cladding on the buildings investigated in the field study, along with the damages to such cladding, were mapped and discussed. Approximately 58% of buildings with floor underside cladding had damages to these components. Evidence of damage was found

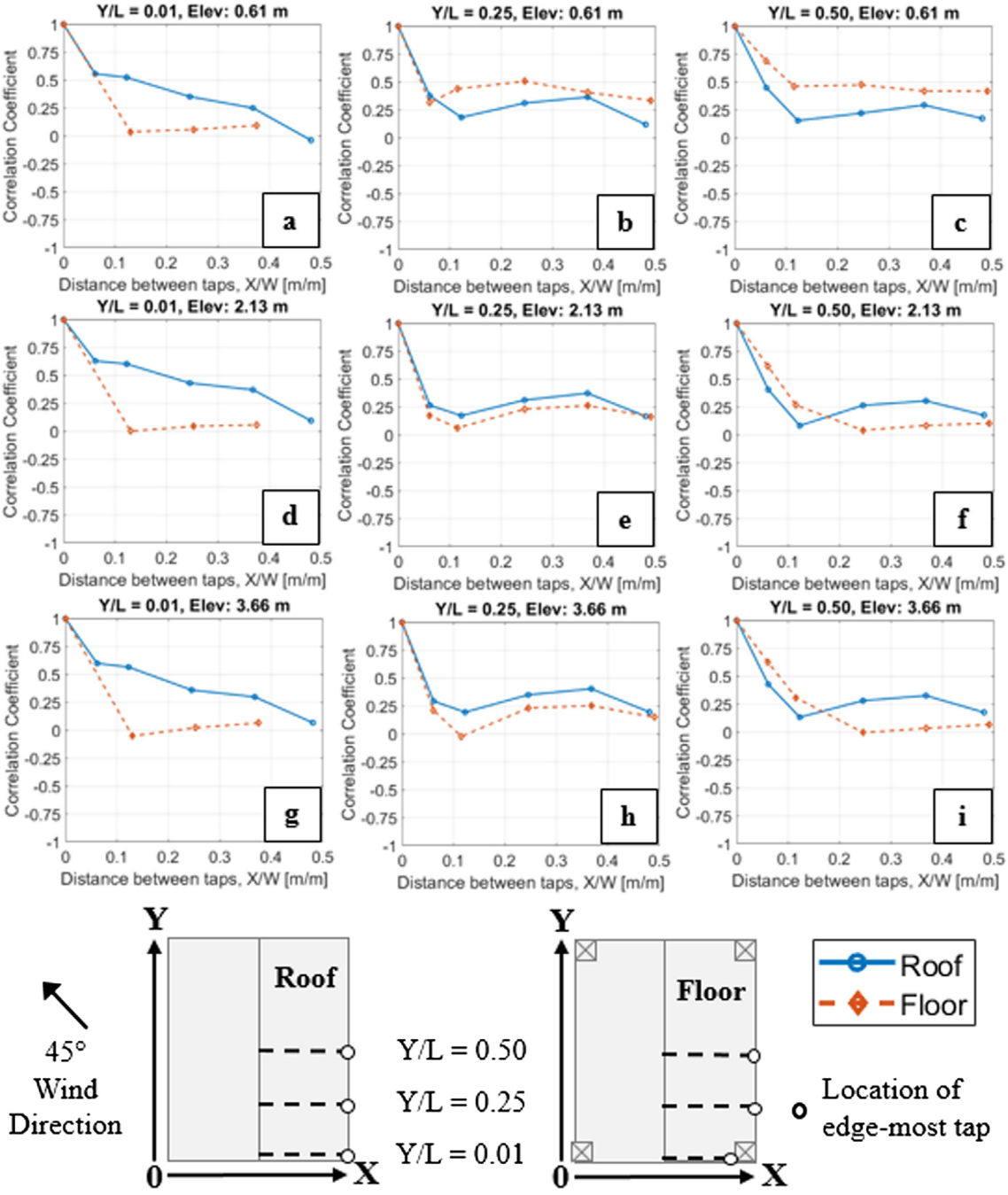

Fig. 20. Correlation coefficients between the edge-most tap and taps at increasing distances along a horizontal width cross-section, where both taps exist on either the roof or floor of the model, for a wind direction 45° to roof ridge.

at all three wind speed ranges considered (193–241 km/h, overall), and, critically, in the cases where storm surge floodwaters did not reach the floor underside.

According to the wind tunnel results, roof pressure coefficients on the elevated models did not change considerably compared to the non-elevated case. However, evidence of significant peak floor underside pressures were found. Pressure coefficients were especially high along the edges of the building and directly adjacent to the corner stilts when the building models were elevated to the scale equivalent of 2.13 m and 3.66 m, in some particular cases surpassing those on the roof at the same relative location by nearly 60%. At these building elevations, regions of extremely high negative pressure coefficients near the edges of the building were identified, while such regions were not observed in the 0.61 m elevation case. In general, floor underside maximum peak pressure coefficients were lower than those on the roof; the same was the case for the pressure coefficients across the floor underside when compared to those on the gable roof. However, they remain substantial enough to require proper and deliberate consideration during design, especially given that the recorded floor pressure time-histories had noticeably higher correlations with one-another over greater distances compared to those recorded on the roof.

Common trends were identified between the field study observations and the experimental results. Damages to the floor cladding near the edges of the buildings were frequent, patterns of which are backed by the presence of critical negative pressure coefficients in the wind tunnel data. Further commonalities are suggested between observations of widespread floor cladding damage and the relatively high correlation coefficients for the floor underside. Thus, concluding, more work is

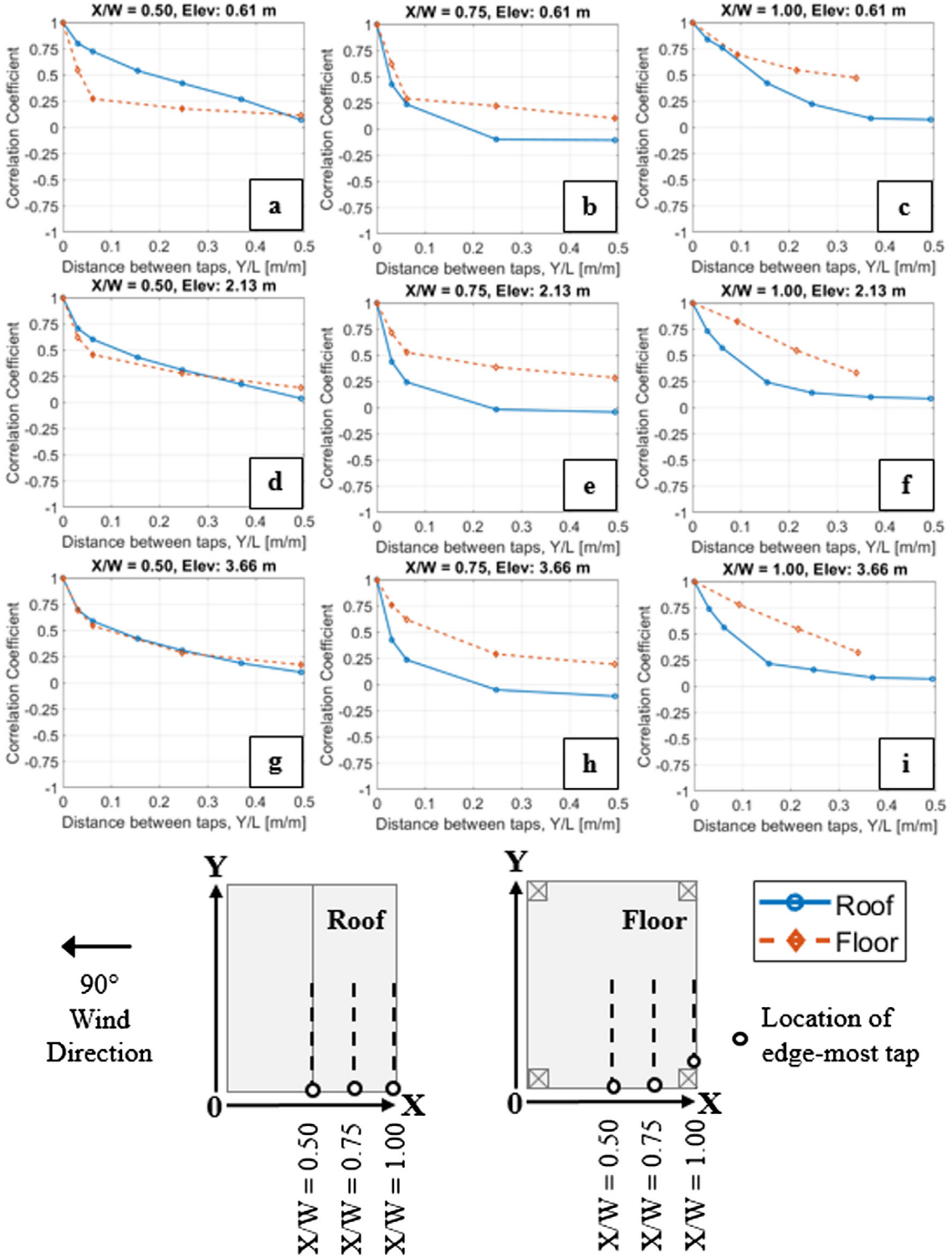

Fig. 21. Correlation coefficients between the edge-most tap and taps at increasing distances along a horizontal length cross-section, where both taps exist on either the roof or floor of the model, for a wind direction perpendicular to roof ridge.

needed both in research and with immediate translation into practice.

CRediT authorship contribution statement

Jae H. Kim: Conceptualization, Methodology, Software, Formal analysis, Investigation, Data curation, Writing - original draft, Writing - review & editing, Visualization. **Mohammadtaghi Moravej:** Conceptualization, Methodology, Software, Formal analysis, Investigation, Resources, Data curation, Writing - review & editing, Visualization. **Elaina J. Sutley:** Conceptualization, Methodology, Investigation, Resources, Data curation, Writing - review & editing, Visualization, Supervision, Project administration, Funding acquisition. **Arindam Chowdhury:** Conceptualization, Methodology, Investigation, Resources, Data curation, Writing - review & editing, Supervision, Project administration, Funding acquisition. **Thang N. Dao:** Conceptualization, Investigation, Resources, Writing - review & editing,

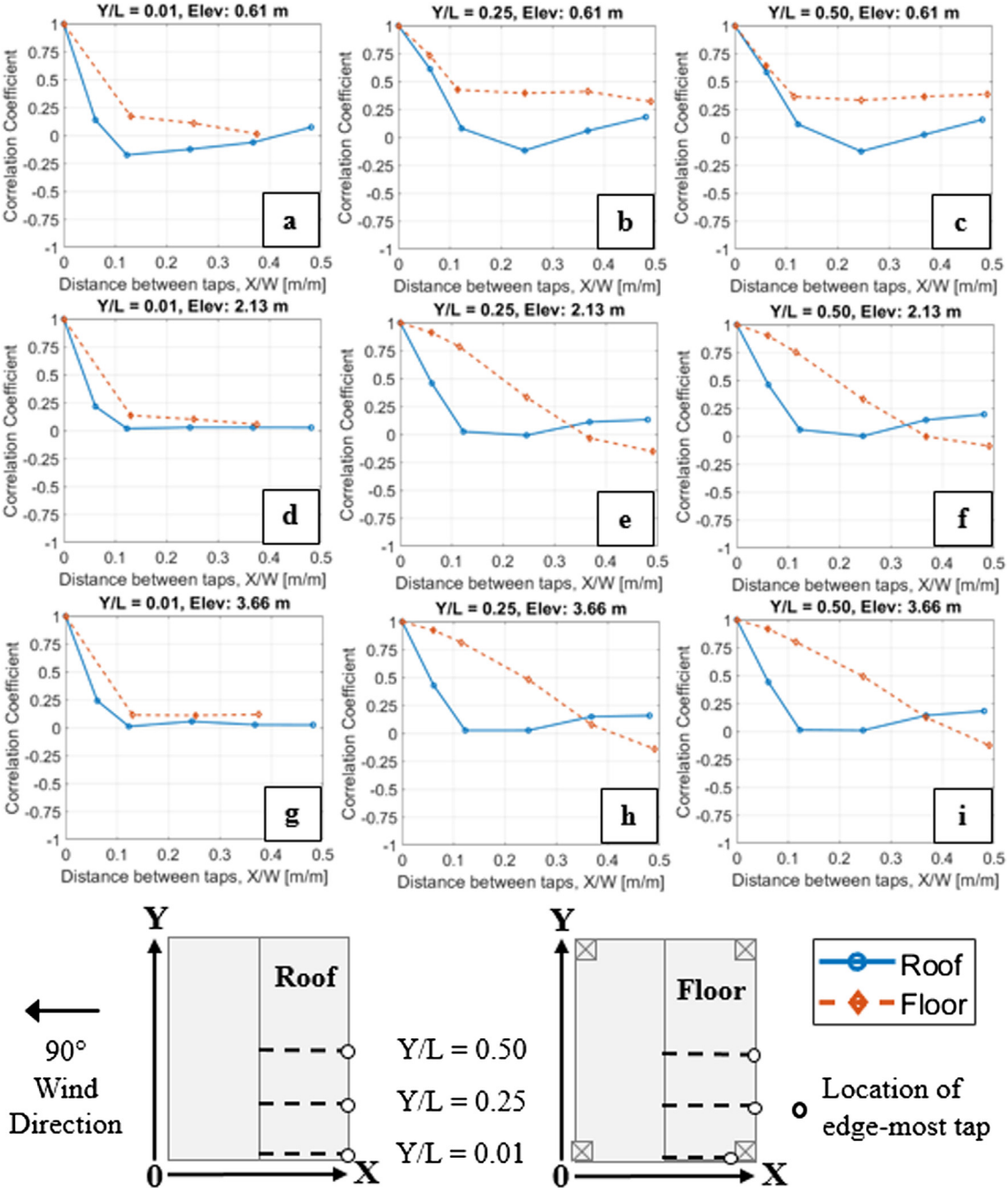

Fig. 22. Correlation coefficients between the edge-most tap and taps at increasing distances along a horizontal width cross-section, where both taps exist on either the roof or floor of the model, for a wind direction perpendicular to roof ridge.

Project administration.

Declaration of Competing Interest

The authors declare that they have no known competing financial interests or personal relationships that could have appeared to influence the work reported in this paper.

Acknowledgements

The field reconnaissance and analysis work presented here was supported by the National Science Foundation (NSF) under Award CMMI-1903486. The authors gratefully acknowledge this support. Any opinions, findings, and conclusions or recommendations expressed in this material are those of the authors and do not necessarily reflect the views of the National Science Foundation.

The experimental testing was part of a larger project supported by the State of Florida Department of Emergency Management awarded to the fourth author. The experiments were performed at the NHERI Wall of Wind Experimental Facility (WOW EF) supported by the NSF (Award #1520853). All authors gratefully acknowledge these supports and data access for the purposes of this paper.

Appendix A. Supplementary material

Supplementary data to this article can be found online at https://doi.org/10.1016/j.engstruct.2020.111101.

References

[1] Vann WP, McDonald JR. Engineering analysis: mobile homes in windstorms. Institute for Disaster Research, Texas Tech University, Lubbock, TX; 1978.

[2] Peacock WG, Morrow BH, Gladwin H. Hurricane Andrew: ethnicity, gender, and the sociology of disaster. London: Routledge; 1997.

[3] Highfield WE, Peacock WG, Van Zandt S. Mitigation planning: Why hazard exposure, structural vulnerability, and social vulnerability matter. J Plann Educ Res 2014;34(3):287–300.

[4] Tomiczek T, Kennedy A, Rogers S. Survival analysis of elevated homes on the Bolivar Peninsula after Hurricane Ike. In: Conference on advances in hurricane engineering 2012, ATC & SEI, Miami, FL, USA; 2012. p. 108–18.

[5] Marshall RD. The measurement of wind loads on a full-scale mobile home. NBSIR 77-1289, National Bureau of Standards, Washington, DC; 1977.

[6] Roy RJ. Wind tunnel measurements of total loads on a mobile home. J Wind Eng Ind Aerodyn 1983;13(1–3):327–38.

[7] Holmes JD. Wind pressures on tropical housing. J Wind Eng Ind Aerodyn 1994;53(1–2):105–23.

[8] Liu J, Niu K, Mak CM, Xia Q. Detached eddy simulation of pedestrian-level wind and gust around an elevated building. Build Environ 2017;125:168–79.

[9] Yun CB, Abdelrahman AM, Wang PC. Along-wind gust effect on elevated structures. Eng Struct 1979;1(3):121–4.

[10] Moravej M, Irwin P, Zisis I, Chowdhury AG, Hajra B. Effects of roof heights on local pressure and velocity coefficients on building roofs. Eng Struct 2017;150:693–710.

[11] American Society of Civil Engineers (ASCE). Minimum design loads for buildings and other structures. ASCE/SEI 7-16, Reston, VA; 2017.

[12] ASCE. Minimum design loads for buildings and other structures. ANSI/ASCE 7-88, Reston, VA; 1990.

[13] Federal Emergency Management Agency (FEMA). Coastal construction manual, 4th ed. FEMA P-55, Dept. of Homeland Security; 2011. https://www.fema.gov/media-library/assets/documents/3293 [Jan. 17, 2018].

[14] National Oceanic and Atmospheric Administration (NOAA). Data in GIS formats. National Hurricane Center and Central Pacific Hurricane Center; 2019 [accessed June 1, 2019]. https://www.nhc.noaa.gov/data/tcr/index.php?season=2018&basin=atl.

[15] Coastal Emergency Risks Assessment (CERA). Maximum water height above NAVD88, hindcast storm MICHAEL, track: NHC best track, 06-Oct – 12-Oct 2018; 2019. https://cera.coastalrisk.live/ [May 27, 2019].

[16] Sutley EJ, Dao T, Kim JH. RAPID: assessing the performance of elevated wood buildings, including manufactured housing, in Florida during 2018 Hurricane Michael. Dataset DesignSafe-CI 2019. https://doi.org/10.17603/ds2-85fv-n684.

[17] Chowdhury AG, Zisis I, Irwin P, Bitsuamlak G, Pinelli J-P, Hajra B, et al. Large-scale experimentation using the 12-fan Wall of Wind to assess and mitigate hurricane wind and rain impacts on building and infrastructure systems. J Struct Eng 2017;143(7):04017053.

[18] Kopp GA, Morrison MJ, Henderson DJ. Full-scale testing of low-rise, residential buildings with realistic wind loads. J Wind Eng Ind Aerodyn 2012;104–106:25–39.

[19] ESDU. Characteristics of atmospheric turbulence near the ground. Part II: single point data for strong winds (neutral atmosphere). ESDU 85020, London, UK; 2002.

[20] Irwin HPAH, Cooper KR, Girard R. Correction of distortion effects caused by tubing systems in measurements of fluctuating pressures. J Wind Eng Ind Aerodyn 1979;5:93–107. https://doi.org/10.1016/0167-6105(79)90026-6.

[21] Stathopoulos T, Surry D. Scale effects in wind tunnel testing of low buildings. J Wind Eng Ind Aerodyn 1983;13(1–3):313–26.

[22] Mooneghi MA, Irwin P, Chowdhury AG. Partial turbulence simulation method for predicting peak wind loads on small structures and building appurtenances. J Wind Eng Ind Aerodyn 2016;157:47–62.

[23] Moravej M. Investigating scale effects on analytical methods of predicting peak wind loads on buildings. Ph.D. Dissertation, Florida International University, Miami, FL; 2018.